NONPROPAGATING EXCITATIONS IN 2-D

by

Ray Gabriel Abney Fiallos

A thesis submitted to the faculty of
The University of North Carolina at Charlotte
in partial fulfillment of the requirements
for the degree of Master of Science in
Applied Physics

Charlotte

2020

Approved by:

_____

Dr. Gregory Gbur

_____

Dr. Thomas Suleski

_____

Dr. Stanislav Molchanov

ABSTRACT

RAY GABRIEL ABNEY FIALLOS. Nonpropagating Excitations in 2-D. (Under the direction of DR. GREGORY GBUR)

Nonpropagating excitations have been studied in 1-D and in 3-D, but not so much in 2-D. So, this thesis concerns 2-D nonpropagating excitations. In particular, we construct nonpropagating excitations confined to an annulus under a time-independent scheme, and then we construct nonpropagating excitations confined to a sector of an annulus under a time-dependent scheme. In the time-dependent scheme, we have our nonpropagating excitation orbit the center of our annulus, demonstrating for the first time a nonpropagating excitation with significant translational motion.

In this thesis, we also reproduce the results of a 2009 paper involving 1-D nonpropagating excitations, and we extend the theory in this 2009 paper concerning 1-D nonpropagating excitations to 2-D nonpropagating excitations.

DEDICATION

I would like to dedicate this thesis to my mother Patricia Abney. She is the one who pushed me to get through school; and without her, I would not have made it this far. I would also like to dedicate this thesis to all of my teachers and all the other people who make and have made my education possible.

ACKNOWLEDGEMENTS

I would like to acknowledge Dr. Gregory Gbur, my graduate advisor who helped me with the experiments mentioned in this thesis and in the editing process. His help was indispensable.

TABLE OF CONTENTS

LIST OF FIGURES vii

CHAPTER 1: INTRODUCTION 1

CHAPTER 2: THE 1-D SCHEME 4

2.1. Theory 4

2.2. The Amplitude Construction Method 6

2.3. The Force Construction Method 9

CHAPTER 3: THE 2-D TIME-INDEPENDENT SCHEME 14

3.1. Theory 14

3.2. Computations 16

CHAPTER 4: THE 2-D TIME-DEPENDENT SCHEME 24

4.1. Theory 24

4.2. Computations 26

CHAPTER 5: CONCLUSIONS 36

REFERENCES 37

APPENDIX: WHEN THE HANKEL FUNCTION'S ARGUMENT IS ZERO 39

LIST OF FIGURES

FIGURE 2.1: A nonpropagating excitation and corresponding force created by the amplitude construction method. 8

FIGURE 2.2: A directional excitation and its corresponding force distribution created by the amplitude construction method. 9

FIGURE 2.3: An illustrative example of a force distribution $q(x)$ to be used in the force construction method. 10

FIGURE 2.4: Nonpropagating excitations created with the force construction method. 12

FIGURE 2.5: The real part of a directional excitation created from the force distribution $q(x)$, a complex-valued function. 13

FIGURE 3.1: Nonpropagating excitations on annuli with inner radii $a = 0, 1$ and outer radius $b = 3$, plotted against r with $\theta = 0$. 18

FIGURE 3.2: 3-D Plots of nonpropagating excitations on annuli with inner radii $a = 0, 1$ and outer radius $b = 3$. 19

FIGURE 3.3: The forces corresponding with various nonpropagating excitations on annuli with inner radii $a = 0, 1$ and outer radius $b = 3$, plotted against r with $\theta = 0$. 20

FIGURE 3.4: The approximations of our nonpropagating excitations on annuli with inner radii $a = 0, 1$ and outer radius $b = 3$. 22

FIGURE 4.1: The contour plot of a nonpropagating excitation and its Fourier series. 28

FIGURE 4.2: The orbits about the center of an annulus of a nonpropagating excitation and its corresponding force. 29

FIGURE 4.3: Plots of nonpropagating excitations confined to a sector of an annulus. 30

FIGURE 4.4: Plots of the Fourier series of our nonpropagating excitations of Figure 4.3. 31

FIGURE 4.5: The plots of the forces corresponding with the nonpropagating excitations of Figure 4.3 32

FIGURE 4.6: An illustration of the ripple pattern created by the use of a Fourier series. 34

FIGURE 4.7: The invariance in the form of a force distribution with respect to the shape of the sector of our annulus. 35

FIGURE 1: A section D_j of a larger region D over which a Green's formula is calculated. 40

CHAPTER 1: INTRODUCTION

When a driving force is applied to a bounded region on, say, a string, one would expect waves to propagate from the region being excited; but this does not necessarily have to happen. Under certain circumstances when a driving force is applied to a bounded region, a wave results only within this bounded region with no disturbance being found outside. Under these circumstances, that which creates our driving force is known as a *nonradiating source* and the wave that results is known as a *nonpropagating excitation*. (Note that in some literature, it is the driving force itself that is defined as the nonradiating source. The term nonradiating source can be used interchangeably for either the driving force or for whatever is creating the driving force.)

In this paragraph and in the couple that follow, we draw from two writings [1, 2] of Gbur our brief discussion of the history of the study of nonpropagating excitations and why the study of nonpropagating excitations is important. In the early 1900's, Sommerfeld and other scientists first put forth theories concerning the extended rigid electron. Then in 1910, Ehrenfest in his paper [3] was the first researcher to recognize that these charge distributions considered by Sommerfeld and others could oscillate in certain ways and not radiate. Later, in 1933, Schott showed in [4] how it is possible for a spherically charged shell to move in a periodic orbit, namely to move about in a wobbling sort of motion, without radiating. In 1948, Bohm and Weinstein showed in [5] that certain rigid charge distributions can oscillate and not radiate, even in the absence of all forces other than their own retarded fields. In 1964, Goedecke in [6] derived a criterion for absence of radiation from arbitrary time-periodic charge-current distributions. In his paper, Goedecke also demonstrated that it is possible to

have an asymmetric, spinning, extended charge distribution that does not radiate.

Some of the scientists who studied nonpropagating excitations and nonradiating sources believed that nonradiating charge distributions could be used as models for elementary particles. Schott suggested in [4] that nonradiating charge distributions could make for a stable model of the neutron and other atomic nuclei. Bohm and Weinstein suggested in [5] that some kinds of mesons could be electrons in a particular excited state of self-oscillation, with the electrons being the nonradiating sources. And Goedecke suggested in [6] that, from theory concerning nonradiating charge distributions, there could arise a "theory of nature" in which all stable particles are "nonradiating charge-current distributions whose mechanical properties are electromagnetic in origin."

The existence (or nonexistence) of nonradiating sources is also important to the solution of the inverse source problem. The term *inverse source problem* is defined in [2] as "the determination of the properties of a radiation source from measurements of the field radiated by that source." In 1973, Friedlander wrote [7], a paper in which he discussed the mathematics of nonradiating sources and the inverse source problem. Also in 1973, Devaney and Wolf gave necessary and sufficient conditions for monochromatic current distributions to be nonradiating in their paper [8]. And in 1977, Bleistein and Cohen in [9] concluded that inverse source problems are nonunique whenever their corresponding direct problems admit nonradiating sources.

In more recent times, we have the studies of [10, 11, 12], which all concern nonpropagating excitations in 1-D. These three papers were written between 1998 and 2009. Some of these papers, namely [11, 12], specifically talk about nonpropagating excitations on long strings. Published in 2003, [1] discusses nonpropagating excitations and invisibility. And written within the last five years, we have [13, 14, 15], all of which concern nonradiating anapoles. The authors of [15] make use of the theorems found in [8].

Nonpropagating excitations in 1-D and in 3-D have been covered in the literature, but 2-D nonpropagating excitations have not been studied in detail. ([2] gives a little bit of discussion about 2-D nonpropagating excitations; but, to our knowledge, there is no other literature discussing 2-D nonpropagating excitations.) So, in this thesis, we concern ourselves with nonpropagating excitations in 2-D. This thesis concerns itself mostly with constructing nonpropagating excitations. In Chapter 2, we reproduce and discuss the 1-D results obtained by Moses, Gan, and Gbur in [10]; in Chapter 3, we construct 2-D time-independent nonpropagating excitations confined to an annulus; and in Chapter 4, we construct 2-D time-dependent nonpropagating excitations confined to a sector of an annulus. Up to this point, all studies concerning nonpropagating excitations and nonradiating sources have concerned themselves with monochromatic excitations or very small vibratory motions. But here, and for the first time, we demonstrate a nonpropagating excitation that moves in an orbiting motion, showing translational motion.

CHAPTER 2: THE 1-D SCHEME

In this chapter, we discuss nonpropagating excitations in 1-D. Our discussion in this chapter will draw from [10], the paper published in 2009 by Dylan Moses, Choon How Gan, and Gregory Gbur. In the research for this thesis, the first thing we wanted to do was to reproduce the results of [10]. This said, in Section 2.1 we will discuss the theory of 1-D nonpropagating excitations as put forward by [10]; and in Sections 2.2 and 2.3, we will construct some nonpropagating excitations according to the amplitude construction and force construction methods outlined in [10]. It is upon the theory and work in this chapter that we base our work found in the next two chapters.

2.1 Theory

We first consider an infinitely long string. For waves on this string, we have the wave equation

$$\frac{\partial^2}{\partial x^2}y(x,t) - \frac{1}{v^2}\frac{\partial^2}{\partial t^2}y(x,t) = q(x,t), \tag{2.1}$$

where v is the speed of the wave and $q(x,t)$ is the driving force that creates the wave whose amplitude is $y(x,t)$. Now assume that our driving force is of monochromatic form $q(x,t) = q(x)\exp(-i\omega t)$. Then, at steady state, we have that $y(x,t) = y(x)\exp(-i\omega t)$ and our problem now concerns studying solutions of the 1-D Helmholtz equation

$$\frac{d^2}{dx^2}y(x) + k^2 y(x) = q(x), \tag{2.2}$$

where $k = \omega/v$.

We now consider a closed interval $[a,b]$ on our infinitely long string. From [16], we

have that the solution of equation (2.2) within $[a, b]$ is

$$y(x) = \frac{1}{2ik} \int_a^b q(x') \exp(ik|x - x'|)dx'. \tag{2.3}$$

For $x < a$, equation (2.3) becomes

$$y(x)|_L = \frac{\exp(-ikx)}{2ik} \int_a^b q(x') \exp(ikx')dx'; \tag{2.4}$$

and for $x > b$, equation (2.3) becomes

$$y(x)|_R = \frac{\exp ikx}{2ik} \int_a^b q(x') \exp(-ikx')dx'. \tag{2.5}$$

Equations (2.4) and (2.5) are proportional to the Fourier transform of the force density,

$$\tilde{q}(K) = \int_a^b q(x') \exp(-2\pi iKx')dx'. \tag{2.6}$$

In this chapter, we will concern ourselves with functions $q(x)$ for which we have

$$\tilde{q}(k') = 0 \qquad \text{or} \qquad \tilde{q}(-k') = 0, \tag{2.7}$$

where $k' = k/2\pi$. From equations (2.4) and (2.5), if we have both of the conditions (2.7), then equations (2.4) and (2.5) are both zero and we have a nonpropagating excitation. On the other hand, if we only have one of the conditions of (2.7), then only one of the equations (2.4) and (2.5) is zero and we have what is called a *directional excitation*, a wave that propagates in only one direction but not in the other. For both nonpropagating and directional excitations, these equations demonstrate that the phenomena are the result of a special wave interference effect in which the waves produced by all points in the source region combine to form complete destructive interference.

2.2 The Amplitude Construction Method

From [11], we have that, if $y(x)$ is a nonpropagating excitation, then it will satisfy the boundary conditions

$$y(a) = y(b) = 0, \qquad \left.\frac{dy}{dx}\right|_{x=a} = \left.\frac{dy}{dx}\right|_{x=b} = 0. \tag{2.8}$$

So the amplitude construction method of finding a nonpropagating excitation is to define any function $y(x)$ that would satisfy the boundary conditions (2.8). Once we have our $y(x)$, we put it through our Helmholtz equation (2.2) to determine the nonradiating source $q(x)$ that would generate our $y(x)$.

At this point it would be good to mention that, for the rest of this chapter, we will have $a = -x_0$ and $b = x_0$; the purpose being, as the authors of [10] say, "to easily consider, without any loss of generality, nonpropagating excitations of even and odd symmetry."

We define our nonpropagating excitations as piecewise continuous functions of the form

$$y(x) = \begin{cases} f(x) & x \in [-x_0, x_0], \\ 0 & \text{otherwise}, \end{cases} \tag{2.9}$$

where $f(x)$ is a polynomial of the form

$$f(x) = \sum_{n=0}^{N} c_n x^n, \tag{2.10}$$

where $c_n \in \mathbb{C}$. We need to determine what our c_n's are and how many terms we need for our polynomial $f(x)$. In order for our $y(x)$ as defined by equation (2.9) to fulfill the boundary conditions (2.8), we need $f(x)$ as defined by equation (2.10) to satisfy the conditions (2.8). We try the form

$$f(x) = c_m x^m + c_{m+2} x^{m+2} + c_{m+4} x^{m+4}. \tag{2.11}$$

So putting our $f(x)$ through the boundary conditions (2.8) and then setting $x = x_0$,

we end up with the system of equations

$$\begin{aligned} c_m x_0^m + c_{m+2} x_0^{m+2} + c_{m+4} x_0^{m+4} = 0, \\ m c_m x_0^{m-1} + (m+2) c_{m+2} x_0^{m+1} + (m+4) c_{m+4} x_0^{m+3} = 0. \end{aligned} \tag{2.12}$$

So, solving our system of equations for c_m, c_{m+2}, and c_{m+4} and letting $c_m = A$, $c_{m+2} = B$, and $c_{m+4} = C$; we have $A = Cu_1^4$, $B = -2Cu_1^2$, and our free variable $C = 1$. And, of particular importance are the definitions $u = kx$, $u_0 = -kx_0$, $u_1 = kx_0$, $k = 1/x_0$, and $x_0 = 1$. Thus, $u = x/x_0$.

As for the number of terms in our polynomial in equation (2.11), we need at least three. If, say, we did not have the term $c_{m+4}x^{m+4}$ in our polynomial $f(x)$, then this would give us the system of equations

$$\begin{aligned} c_m x_0^m + c_{m+2} x_0^{m+2} = 0, \\ m c_m x_0^{m-1} + (m+2) c_{m+2} x_0^{m+1} = 0. \end{aligned} \tag{2.13}$$

Our system of equations above only has a nontrivial solution for c_m and c_{m+2} if its determinant equals zero; or, rather, if $2x_0^{2m+1} = 0$. We cannot have $2x_0^{2m+1} = 0$ since $x_0 \neq 0$. Thus, we need at least three terms.

Now, going back to our nonpropagating excitation $y(x)$, which we will redefine in terms of u (like in [10]), from equation (2.9) we get

$$y(u) = \begin{cases} Au^m + Bu^{m+2} + Cu^{m+4} & u \in [u_0, u_1], \\ 0 & \text{otherwise.} \end{cases} \tag{2.14}$$

Then we take our $y(u)$ and put it through our Helmholtz equation to get our $q(u)$ (keeping in mind that there is a second derivative in the Helmholtz equation; which, due to our change of coordinates $u = kx$, requires that we multiply this derivative by k^2). Thus, we arrive at our first reproduced results, as shown in Figure 2.1. These results are identical with the corresponding results obtained in [10].

The amplitude construction method can also be used to create directional excita-

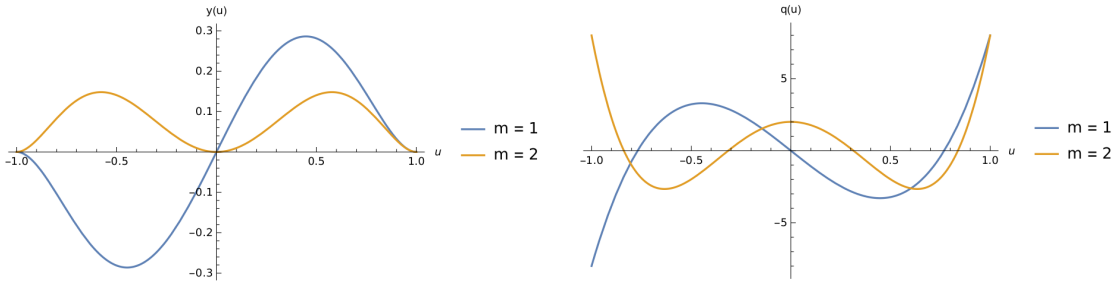

(a) (b)

Figure 2.1: The graphs that result from using the amplitude construction method to generate a nonpropagating excitation. (a) Our nonpropagating excitation $y(u)$ plotted against u for the cases $m = 1$ and $m = 2$. (b) Our nonradiating source $q(u)$ that generates our nonpropagating excitation $y(u)$ above for the cases $m = 1$ and $m = 2$.

tions. Equation (2.4) implies that every wave propagating to the left of $[a, b]$ has the form $y(x)|_L = A_0 \exp(-ikx)$, where $A_0 \in \mathbb{C}$ is a constant. Thus, constructing a (left-going in this case) directional excitation using the amplitude construction method amounts to finding a $y(x)$ such that

$$\begin{aligned} y(x_0) = 0, \qquad & \tfrac{dy}{dx}\big|_{x=x_0} = 0, \\ y(-x_0) = A_0 \exp(ikx_0), \qquad & \tfrac{dy}{dx}\big|_{x=-x_0} = -ikA_0 \exp(ikx_0). \end{aligned} \tag{2.15}$$

Right-going directional excitations are created in a similar fashion.

Thus, we define

$$y(u) = \begin{cases} 0 & \text{if } u \le u_0, \\ A(u-u_1)^m + B(u-u_1)^{m+2} + Ce^{iu} & \text{if } u_0 < u < u_1, \\ Ce^{iu} & \text{if } u \ge u_1. \end{cases} \tag{2.16}$$

Equation (2.16) defines a right-going directional excitation. For equation (2.16), some constants have been redefined. We now choose $k = 4/x_0$. We also have $A = A_R + iA_I$ and $B = B_R + iB_I$ with

$$A_R = \frac{C[2\Delta u \sin u_0 - (m+2)\cos u_0]}{2(-2\Delta u)^m}, \tag{2.17}$$

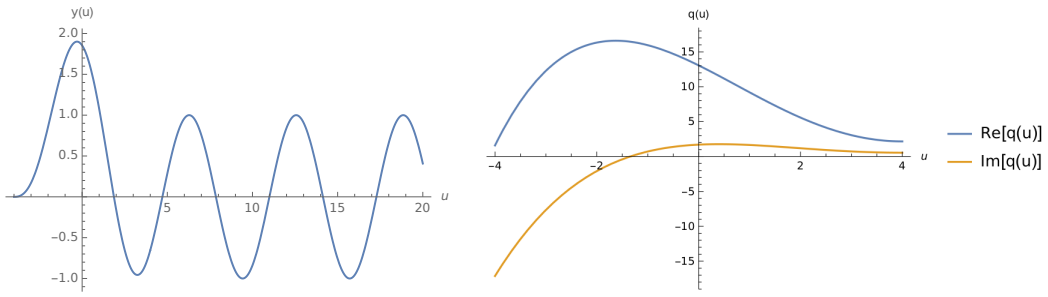

(a) (b)

Figure 2.2: The graphs that result from using the amplitude construction method to generate a directional excitation. (a) Our directional excitation going toward the right. Here, $m = 2$. (b) The real and imaginary parts of our nonradiating source $q(u)$ that generates our graph above.

$$A_I = -\frac{C[2\Delta u \cos u_0 + (m+2)\sin u_0]}{2(-2\Delta u)^m}, \tag{2.18}$$

$$B_R = \frac{C[m\cos u_0 - 2\Delta u \sin u_0]}{2(-2\Delta u)^{m+2}}, \tag{2.19}$$

$$B_I = \frac{C[m\sin u_0 + 2\Delta u \cos u_0]}{2(-2\Delta u)^{m+2}}, \tag{2.20}$$

with $\Delta u = (u_1 - u_0)/2 \neq 0$. C and u are as they were before. Thus, we get the results of Figure 2.2. Note that, while Figure 2.2a is identical with its counterpart in [10], Figure 2.2b is slightly different from its counterpart in [10]. In Figure 2.2b, neither of the graphs go to zero as u approaches 4; but they do in the corresponding graph in [10]. However, the graphs of Figure 2.2b are at least qualitatively the same as the corresponding graph in [10]. This said, seeing that we have meticulously checked our calculations and the *Mathematica* script that created Figure 2.2, we conclude that the figure in [10] corresponding with Figure 2.2b has an error.

2.3 The Force Construction Method

The force construction method creates nonpropagating excitations by taking a nonradiating source $q(x)$ and using equation (2.3) to find the nonpropagating excitation $y(x)$. So, really, it works like the amplitude construction method, but backwards. An advantage of the force construction method is that we can work with sources $q(x)$

that are in principle easier to construct experimentally.

In [10], the authors start off with the step function

$$S(u) = \begin{cases} 1 & \text{if } |u| \leq 1, \\ 0 & \text{if } |u| > 1. \end{cases} \tag{2.21}$$

Using this step function $S(u)$, they construct a nonradiating source

$$q(x) = \sum_{n=1}^{N} a_n S\left(\frac{x - x_n}{\sigma_n}\right), \tag{2.22}$$

where N is the total number of steps in our force distribution $q(x)$, where a_n is the height of the nth step, and where σ_n is the half-width of the nth step, as illustrated in Figure 2.3. A nonpropagating excitation will result for the case $N = 1$ if

$$k\sigma_1 = m\pi, \tag{2.23}$$

where $m \in \mathbb{Z} - \{0\}$ and where k is the wave number of our nonpropagating excitation.

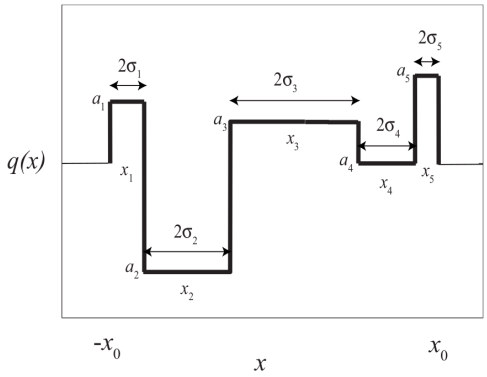

Figure 2.3: A general example of what a plot of $q(x)$ ought to look like, as found in [10]. Here, $q(x)$ is a real-valued function and $N = 5$.

In the case of $2N$ steps, the force is defined as

$$q_{e/o}(x) = \sum_{n=1}^{N} a_n \left[S\left(\frac{x - x_n}{\sigma_n}\right) \pm S\left(\frac{x + x_n}{\sigma_n}\right) \right], \tag{2.24}$$

where the $\pm$ is taken positive if we want an even function or taken negative if we

want an odd function. And we have the Fourier transforms of equation (2.24)

$$\tilde{q}_e(\pm k') = \sum_{n=1}^{N} 4a_n\sigma_n \cos(2\pi k' x_n)\mathrm{sinc}(2k'\sigma_n), \tag{2.25}$$

$$\tilde{q}_o(\pm k') = \pm \sum_{n=1}^{N} 4ia_n\sigma_n \sin(2\pi k' x_n)\mathrm{sinc}(2k'\sigma_n); \tag{2.26}$$

where

$$\mathrm{sinc}(x) = \frac{\sin(\pi x)}{\pi x}. \tag{2.27}$$

We need at least two nonzero a_n in order to satisfy the nonpropagating condition, which will give us four steps for q_o and three steps for q_e.

Thus, our first force distribution $q(x)$ is the even function

$$q_e(x) = \begin{cases} 0 & \text{if } x \in (-\infty, -x_0) \cup (x_0, \infty), \\ a_1 & \text{if } x \in [-x_0, -x_0 + 2\sigma_1) \cup [x_0 - 2\sigma_1, x_0], \\ a_2 & \text{if } x \in [-x_0 + 2\sigma_1, x_0 - 2\sigma_1), \end{cases} \tag{2.28}$$

where $\sigma_1 = x_0/4$; and our second force distribution is the odd function

$$q_o(x) = \begin{cases} 0 & \text{if } x \in (-\infty, -x_0) \cup (x_0, \infty), \\ a_1 & \text{if } x \in [-x_0, -x_0 + 2\sigma_1), \\ a_2 & \text{if } x \in [-x_0 + 2\sigma_1, 0), \\ -a_2 & \text{if } x \in [0, x_0 - 2\sigma_1), \\ -a_1 & \text{if } x \in [x_0 - 2\sigma_1, x_0], \end{cases} \tag{2.29}$$

where $\sigma_1 = x_0/5$. In both cases, we let $a_1 = 1$ and we have $k'x_0 = 1.2$; and to determine our a_2's (which are different for the even and odd cases), we have $\tilde{q}(k') = 0$ and then we solve for a_2 in terms of a_1. This gives us

$$a_2 = a_1\left(1 + \frac{\sin(2\pi k' x_0)}{\sin(2\pi k'(2\sigma_1 - x_0))}\right) \tag{2.30}$$

for $q_e(x)$ and

$$a_2 = a_1\left(1 + \frac{1 - \cos(2\pi k' x_0)}{\cos(2\pi k'(2\sigma_1 - x_0)) - 1}\right) \tag{2.31}$$

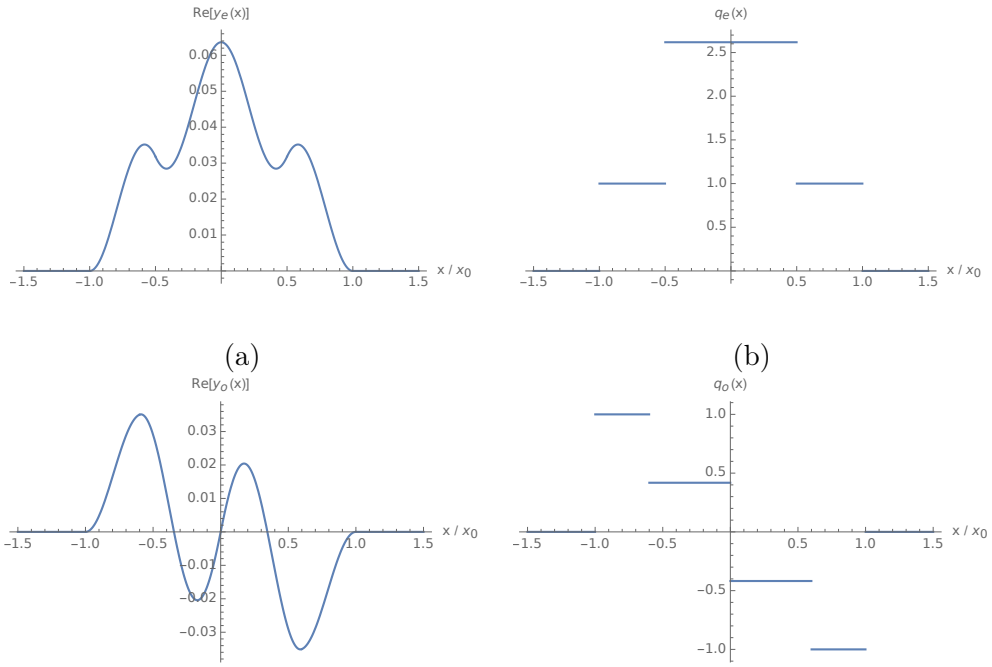

Figure 2.4: (a) The graph of the real part of the $y_e(x)$ that results from using the force construction method on $q_e(x)$. (b) The graph of $q_e(x)$ itself. (c) The graph of the real part of the $y_o(x)$ that results from using the force construction method on $q_o(x)$. (d) The graph of $q_o(x)$ itself.

for $q_o(x)$. Thus, putting $q_e(x)$ and $q_o(x)$ through equation (2.3) to get our corresponding $y_e(x)$ and $y_o(x)$, we get the graphs of Figure 2.4. The graphs of Figure 2.4 are identical with the corresponding graphs found in [10].

And with the force construction method, we can also make directional excitations. Let

$$q(x) = \begin{cases} a_1 + ia_2\text{sgn}(x) & \text{if } -x_0 \leq x \leq x_0, \\ 0 & \text{otherwise,} \end{cases} \tag{2.32}$$

where $\text{sgn}(x)$ is the signum function. We have $\tilde{q}(-k') = 0$ and solve for a_2 in terms of a_1 to get

$$a_2 = \frac{a_1 \sin(2\pi k' x_0)}{\cos(2\pi k' x_0) - 1}. \tag{2.33}$$

Then we have $a_1 = 1$ and $k'x_0 = 1.25$. Thus, using the force construction method on our new $q(x)$, we have the graphs of Figure 2.5. Here we have another instance of our

results not matching the results obtained in [10]. When we enter into *Mathematica* a_2 defined according to equation (2.33), our other constants, and $q(x)$ defined according to equation (2.32); Figures 2.5b and 2.5c are mirror images of the corresponding figures in [10] while Figure 2.5a is identical with the corresponding figure in [10]. Again, we have checked our calculations and our *Mathematica* script and everything looks fine. So there must be another error in [10].

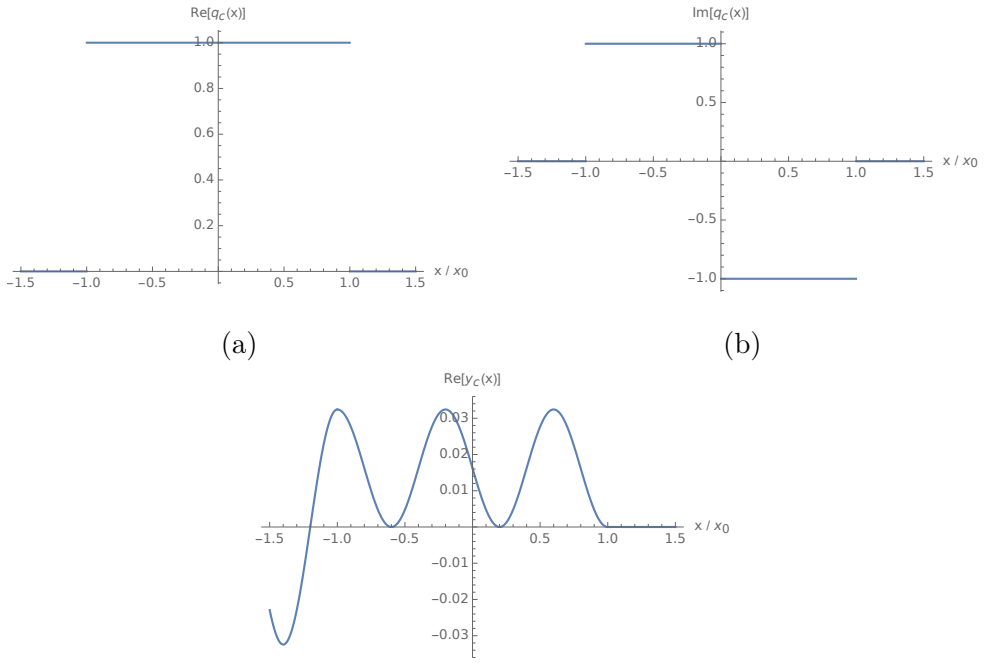

Figure 2.5: (a) The real part of our force, (b) the imaginary part of our force, and (c) the real part of our directional excitation created by our force with the force construction method.

CHAPTER 3: THE 2-D TIME-INDEPENDENT SCHEME

In this chapter, we deal with two-dimensional nonpropagating excitations confined to an annulus. In our research, this was the first new thing we wanted to study. The scenarios studied in this chapter are more realistic and more complex than the 1-D cases, but simpler to calculate than 3-D cases. Furthermore, even-dimensional radiation problems have characteristics that are different from odd-dimensional radiation problems (see Chapter 19 of [17]). This gives us even more reason to study nonpropagating excitations in 2-D. Section 3.1 discusses the theory behind our work and Section 3.2 discusses the numerical experiments we did. Our work in this chapter, namely our work with nonpropagating excitations on an annulus, sets us up to study orbiting nonpropagating excitations in Chapter 4.

3.1 Theory

The two-dimensional wave equation is

$$\nabla^2 U(\mathbf{r},t) - \frac{1}{v^2}\frac{\partial^2}{\partial t^2}U(\mathbf{r},t) = q(\mathbf{r},t), \tag{3.1}$$

where $U(\mathbf{r},t)$ is the displacement of the wave with $\mathbf{r} \in \mathbb{R}^2$, and where, once again, v and $q(\mathbf{r},t)$ are the velocity of the wave and the driving force, respectively. We want to have the monochromatic $U(\mathbf{r},t) = u(\mathbf{r})e^{-i\omega t}$; and this leads us, like in Chapter 2, to concern ourselves with the now two-dimensional Helmholtz equation

$$\nabla^2 u(\mathbf{r}) + k^2 u(\mathbf{r}) = q(\mathbf{r}), \tag{3.2}$$

where k is the wave number. The general solution of equation (3.2), as [17] tells us, is the Green's formula

$$u(\mathbf{r}) = \int_R G(\mathbf{r}, \mathbf{r}')q(\mathbf{r}')d^2\mathbf{r}', \tag{3.3}$$

where R is our region of integration, where

$$G(\mathbf{r}, \mathbf{r}') = i\pi H_0^{(1)}(k|\mathbf{r} - \mathbf{r}'|) \tag{3.4}$$

is the Green's function of the 2-D Helmholtz equation, and where $H_0^{(1)}$ is a Hankel function. Equation (3.3) above is analogous to equation (2.3) of Chapter 2.

To make the math easier, we will be doing most of our work for this chapter in polar coordinates. This means that $u(\mathbf{r}) = u(r, \theta)$, $q(\mathbf{r}) = q(r, \theta)$, and that equation (3.2) becomes

$$\left[\frac{1}{r}\frac{\partial}{\partial r}\left(r\frac{\partial}{\partial r}\right) + \frac{1}{r^2}\frac{\partial^2}{\partial\theta^2}\right] u(r, \theta) + k^2 u(r, \theta) = -4\pi q(r, \theta), \tag{3.5}$$

with the Laplacian

$$\nabla^2 = \frac{1}{r}\frac{\partial}{\partial r}\left(r\frac{\partial}{\partial r}\right) + \frac{1}{r^2}\frac{\partial^2}{\partial\theta^2}. \tag{3.6}$$

This said, we would like to find nonpropagating excitations that are nonzero on the annular domain

$$D = \{(r, \theta)|a \leq r \leq b, 0 \leq \theta \leq 2\pi\}, \tag{3.7}$$

with inner radius a and outer radius b. So finding such nonpropagating excitations amounts to finding functions $u(r, \theta)$ such that the boundary conditions

$$u(a, \theta) = u(b, \theta) = 0, \qquad u_r(a, \theta) = u_r(b, \theta) = 0 \tag{3.8}$$

are satisfied. The boundary conditions (3.8) are analogous to the boundary conditions (2.8) of the previous chapter.

3.2 Computations

Our numerical experiments roughly followed this format: First we defined a function $u(r,\theta)$ satisfying the boundary conditions (3.8). Then, having our $u(r,\theta)$, we put it through equation (3.5) to find our force $q(r,\theta)$. Finally, having our $q(r,\theta)$, we put it through equation (3.3) to reproduce the $u(r,\theta)$ with which we began, confirming that we in fact have a nonpropagating excitation as predicted. So, drawing parallels with our work in Chapter 2, the first part of our experiments for this chapter, the part where we find $q(r,\theta)$ from $u(r,\theta)$, is analogous to the amplitude construction method; and the last part of our experiments, finding $u(r,\theta)$ using $q(r,\theta)$, is like the force construction method. All of the results appearing in this thesis for all of the numerical experiments were computed with *Mathematica*.

In our numerical experiments, we tested four functions that were all based on polynomials. All of these functions followed the general form

$$u(r,\theta) = \begin{cases} f(r) & \text{if } r \in [a,b], \\ 0 & \text{otherwise.} \end{cases} \tag{3.9}$$

So, in defining these functions $u(r,\theta)$, we needed to find functions $f(r)$ that satisfy the boundary conditions (3.8).

It is easy enough to find functions $f(r)$ for our $u(r,\theta)$'s. All we have to do is to follow the approach taken in Chapter 2. First, we let

$$f(r) = c_m(r-K)^m + c_{m+2}(r-K)^{m+2} + c_{m+4}(r-K)^{m+4}, \tag{3.10}$$

where

$$K = \frac{a+b}{2}. \tag{3.11}$$

Then we put our $f(r)$ through the boundary conditions (3.8) so that we have the

system of equations

$$c_m\left(\frac{a-b}{2}\right)^m + c_{m+2}\left(\frac{a-b}{2}\right)^{m+2} + c_{m+4}\left(\frac{a-b}{2}\right)^{m+4} = 0, \tag{3.12}$$

$$mc_m\left(\frac{a-b}{2}\right)^{m-1} + (m+2)c_{m+2}\left(\frac{a-b}{2}\right)^{m+1} + (m+4)c_{m+4}\left(\frac{a-b}{2}\right)^{m+3} = 0, \tag{3.13}$$

where we would like to solve for the coefficients c_m, c_{m+2}, and c_{m+4}. Solving, we get

$$c_m = c_{m+4}\frac{(a-b)^4}{16}, \qquad c_{m+2} = -c_{m+4}\frac{(a-b)^2}{2}, \tag{3.14}$$

and our free variable $c_{m+4} = 1$. Thus, we have an $f(r)$ to substitute into equation (3.9) so as to create our $u(r,\theta)$'s.

In our experiments, the first thing we do is define our constants. In all of our experiments, we always have for our outer radius $b = 3$. For the inner radius, we test for $a = 0, 1$; and we also test for $m = 0, 1$. Since our $u(r,\theta)$'s depend on the values a and m, this thus gives us four $u(r,\theta)$'s to test. We denote the $u(r,\theta)$ with $m = 0$ as $u_0(r,\theta)$, and we denote the $u(r,\theta)$ with $m = 1$ as $u_1(r,\theta)$. Figure 3.1 shows $u_0(r,\theta)$ and $u_1(r,\theta)$ plotted against r with $\theta = 0$ for $a = 0, 1$, and Figure 3.2 gives 3-D plots of these same functions for $a = 0, 1$.

Next we put our functions through equation (3.5) to get our forces $q_0(r,\theta)$ and $q_1(r,\theta)$, corresponding with $u_0(r,\theta)$ and $u_1(r,\theta)$, respectively. In all of our experiments, we put for convenience $k = 1$ as our wave number. Now, when we put our functions through equation (3.5), *Mathematica* will, in the case of $q_0(r,\theta)$ and $a = 1$ for example, give us a result like

$$q_0(r,\theta) = -\frac{1}{4\pi}\begin{cases} \text{Indeterminate} & r = 1 \text{ or } r = 3 \\ 97 - \frac{24}{r} - 96r + 38r^2 - 8r^3 + r^4 & 1 < r < 3 \\ 0 & \text{True.} \end{cases} \tag{3.15}$$

This was a problem we were calculating $q_0(r,\theta)$ and $q_1(r,\theta)$. This problem arises because the second derivative in the Helmholtz equation is discontinuous. To resolve

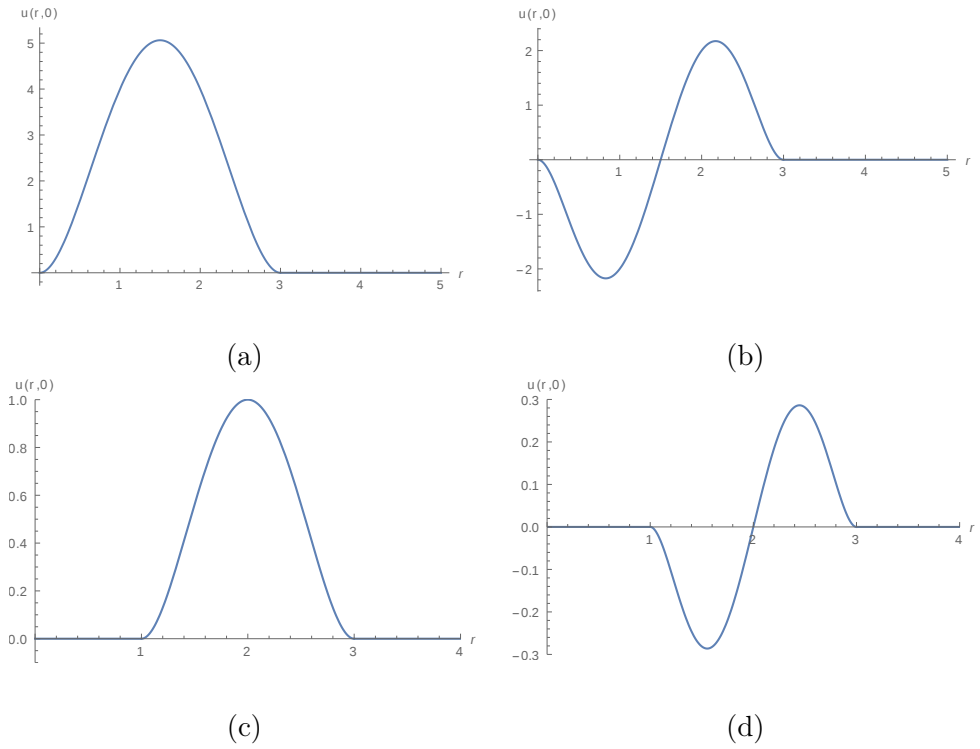

Figure 3.1: Plotted against r with $\theta = 0$, (a) $u_0(r,\theta)$ with $a = 0$, (b) $u_1(r,\theta)$ with $a = 0$, (c) $u_0(r,\theta)$ with $a = 1$, and (d) $u_1(r,\theta)$ with $a = 1$.

this issue, we just substitute "Indeterminate" with a 0; and we are allowed to make such a substitution because for all of our forces, regardless of the values of a or m, we have

$$\lim_{r\to a^-} q(r,\theta) = \lim_{r\to b^+} q(r,\theta) = 0. \tag{3.16}$$

Thus, after making the appropriate substitutions, we get for $a = 0$ the forces

$$q_0(r,\theta) = -\frac{1}{4\pi}\begin{cases} r^4 - 6r^3 + 25r^2 - 54r + 36 & 0 < r < 3 \\ 0 & \text{elsewhere,} \end{cases} \tag{3.17}$$

and

$$q_1(r,\theta) = -\frac{1}{4\pi}\begin{cases} r^5 - \frac{15r^4}{2} + 43r^3 - \frac{267r^2}{2} + 162r - 54 & 0 < r < 3 \\ 0 & \text{elsewhere;} \end{cases} \tag{3.18}$$

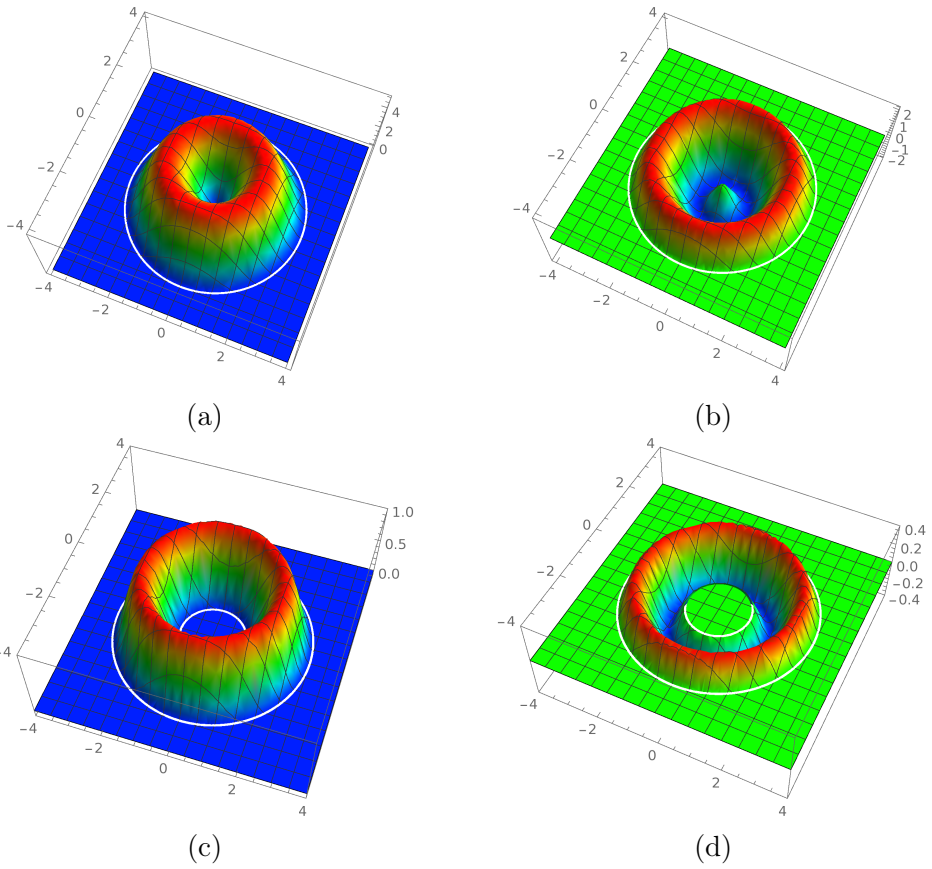

(a) (b)

(c) (d)

Figure 3.2: (a) $u_0(r,\theta)$ with $a=0$, (b) $u_1(r,\theta)$ with $a=0$, (c) $u_0(r,\theta)$ with $a=1$, and (d) $u_1(r,\theta)$ with $a=1$.

and we get for $a=1$ the forces

$$q_0(r,\theta) = -\frac{1}{4\pi}\begin{cases} r^4 - 8r^3 + 38r^2 - 96r - \frac{24}{r} + 97 & 1 < r < 3 \\ 0 & \text{elsewhere,} \end{cases} \tag{3.19}$$

and

$$q_1(r,\theta) = -\frac{1}{4\pi}\begin{cases} r^5 - 10r^4 + 63r^3 - 228r^2 + 399r + \frac{57}{r} - 290 & 1 < r < 3 \\ 0 & \text{elsewhere.} \end{cases} \tag{3.20}$$

Figure 3.3 shows the graphs of our two forces for $a=0,1$. Note the discontinuity in each of the graphs of Figure 3.3.

This is the point where we use our forces $q(r,\theta)$ to reproduce our nonpropagating

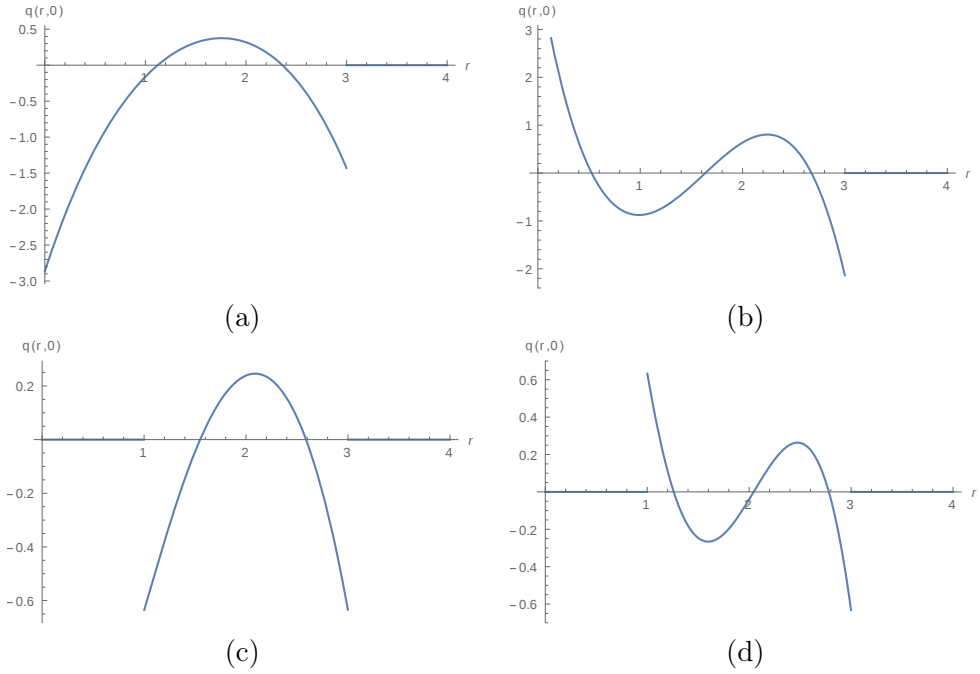

Figure 3.3: Plotted against r with $\theta = 0$, (a) $q_0(r,\theta)$ with $a = 0$, (b) $q_1(r,\theta)$ with $a = 0$, (c) $q_0(r,\theta)$ with $a = 1$, and (d) $q(r,\theta)$ with $a = 1$.

excitations $u(r,\theta)$. Thus, we define our Green's function

$$G(x,y,x',y') = i\pi H_0^{(1)}\left(k\sqrt{(x-x')^2+(y-y')^2}\right). \tag{3.21}$$

Since our forces are functions of r and θ, to convert a point (x,y) in Cartesian coordinates to a point (r,θ) in polar coordinates, we keep in mind the conversions

$$r = \sqrt{x^2+y^2}, \qquad \theta = \text{atan2}(y,x). \tag{3.22}$$

Now, in the case of $a = 0$, we have instances where both arguments of $\text{atan2}(y,x)$ are zero, which will result in *Mathematica* giving us an error message. So, in the case of $a = 0$, instead of having $\theta = \text{atan2}(y,x)$, we have $\theta = 0$. From the definitions of our forces $q(r,\theta)$ in equations (3.17) through (3.20), we are allowed to make such a substitution since our forces do not actually depend on θ. From here, we define our

integrand

$$I(x,y,x',y') = \begin{cases} 0 & \text{if } |\mathbf{r}'| < a \text{ or } |\mathbf{r}'| > b, \\ A(x,y,x',y') & \text{if } |\mathbf{r}-\mathbf{r}'| > 0 \text{ and } a \le |\mathbf{r}'| \le b, \\ B(x,y,x',y') & \text{if } |\mathbf{r}-\mathbf{r}'| = 0 \text{ and } a \le |\mathbf{r}'| \le b; \end{cases} \tag{3.23}$$

where

$$A(x,y,x',y') = G(x,y,x',y')q(\sqrt{(x')^2+(y')^2}, \text{atan2}(y',x')) \tag{3.24}$$

and

$$B(x,y,x',y') = \frac{4.43i}{\sqrt{k\Delta x}} q(\sqrt{(x')^2+(y')^2}, \text{atan2}(y',x')), \tag{3.25}$$

and where

$$|\mathbf{r}'| = \sqrt{(x')^2+(y')^2}, \qquad |\mathbf{r}-\mathbf{r}'| = \sqrt{(x-x')^2+(y-y')^2}. \tag{3.26}$$

We accordingly swap the terms $\text{atan2}(y,x)$ with 0 in the case $a = 0$. Now, as the reader may have observed, when $|\mathbf{r}-\mathbf{r}'| = 0$, we substitute our Green's function with the term $4.43i/\sqrt{k\Delta x}$, where the purpose of the term Δx will be explained momentarily. The reason for this substitution is that the Hankel function blows up when $|\mathbf{r}-\mathbf{r}'| = 0$.

And then we finally calculate our Green's formula equation (3.3) by approximating our continuous integral by a sum over a finite grid. We calculate our Green's formula discretely for every node on a square grid that is 8 units on a side. The distance between nodes going in the x-direction is Δx and the distance between nodes going in the y-direction is Δy. At a point (x_i, y_i), we denote the value of our Green's function to be $u^G(x_i, y_i)$. Thus, at a point (x_i, y_i), we have

$$u^G(x_i,y_i) = \sum_{m=1}^{N}\sum_{n=1}^{N} I(x_i,y_i,x'_m,y'_n)\Delta x'\Delta y', \tag{3.27}$$

where $\Delta x' = \Delta y' = 0.05$ and where $N = 8/\Delta x' = 8/\Delta y'$. Here, $\Delta x' = \Delta x$ and $\Delta y' = \Delta y$. We need to have our values of $\Delta x, \Delta y$ small so that way we can have a

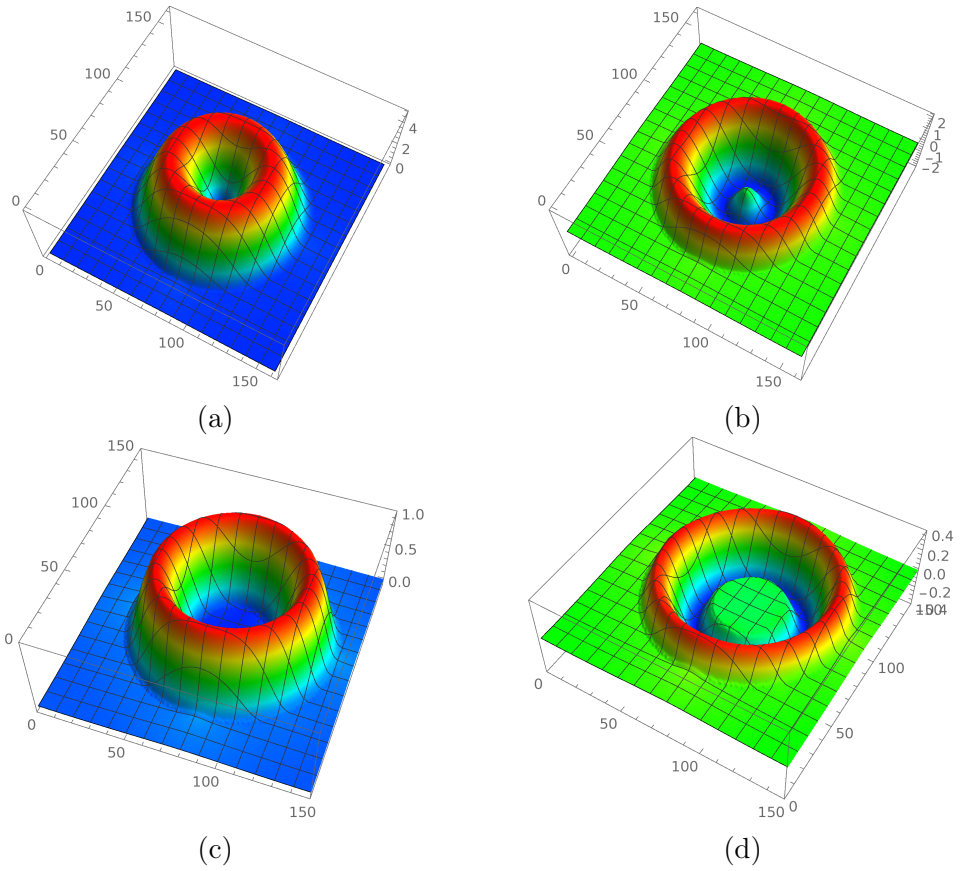

Figure 3.4: (a) $u_0^G(x,y)$ with $a=0$, (b) $u_1^G(x,y)$ with $a=0$, (c) $u_0^G(x,y)$ with $a=1$, and (d) $u_1^G(x,y)$ with $a=1$.

good approximation of our Green's formulae.

And in Figure 3.4 we have our $u^G(x,y)$'s plotted. Note the similarity between the graphs of our Green's formulae and the graphs of the functions $u(r,\theta)$ our Green's formulae are supposed to represent. Thus, we have reproduced our nonpropagating excitations $u(r,\theta)$ and verified that our construction method produces genuine nonpropagating excitations.

Now, most of the results obtained for this thesis were obtained easily enough with a Raspberry Pi 3 Model B computer, the same computer used to write this thesis. But, while the *Mathematica* script used to obtain the results of this chapter were written on this little computer, calculating any of the Green's formulae for our $u(r,\theta)$'s was just too big a job even for a standard desktop computer. So the Green's formulae for

our four $u(r, \theta)$'s and their corresponding graphs found in Figure 3.4 were calculated using a server computer belonging to the Department of Mathematics and Statistics of UNCC. Even using this server computer, it still takes about a day to obtain the results for one or two $u(r, \theta)$'s.

CHAPTER 4: THE 2-D TIME-DEPENDENT SCHEME

After having created nonpropagating excitations confined to an annulus, we wanted to create nonpropagating excitations that were confined to a sector of an annulus. Not only that, but we wanted this nonpropagating excitation to orbit the center of our annulus; and for various nonpropagating excitations $u(r, \theta, t)$, we wanted to determine their corresponding forces $q(r, \theta, t)$. Up to this point, the nonpropagating excitations considered in other literature have involved oscillations in place or wobbling motions like in the case of Schott's spherical shell mentioned in [4]. But the nonpropagating excitations considered in this chapter are different from all others previously considered in other literature because ours experience translational motion. In Section 4.1 we discuss the theory behind our work and in Section 4.2 we discuss the numerical experiments we did.

Now, the reader may be a bit confused. The reader, from our definition of nonpropagating excitation in Chapter 1, may be under the impression that nonpropagating excitations do not move, let alone orbit around the center of an annulus. The excitations of this chapter still constitute nonpropagating excitations because these excitations are confined only to the regions where their respective forces are applied. The only difference now is that the forces are moving around.

4.1 Theory

Let

$$S = \{(r, \theta) | a \leq r \leq b, \phi \leq \theta \leq \psi\} \tag{4.1}$$

be the sector of our annulus

$$D = \{(r, \theta) | a \leq r \leq b, 0 \leq \theta \leq 2\pi\} \tag{4.2}$$

to which we would like to confine our nonpropagating excitation $u(r,\theta)$. Thus, the problem of Chapter 3, the problem defined by equations (3.5) and (3.8), becomes

$$\left[\frac{1}{r}\frac{\partial}{\partial r}\left(r\frac{\partial}{\partial r}\right)+\frac{1}{r^2}\frac{\partial^2}{\partial\theta^2}\right]u(r,\theta)+k^2u(r,\theta)=-4\pi q(r,\theta), \tag{4.3}$$

$$u(a,\theta)=u(b,\theta)=0, \qquad u_r(a,\theta)=u_r(b,\theta)=0, \tag{4.4}$$

$$u(r,\phi)=u(r,\psi)=0, \qquad u_\theta(a,\phi)=u_\theta(r,\psi)=0. \tag{4.5}$$

From our work in Chapter 3, finding a function $u(r,\theta)$ satisfying equations (4.3) and (4.4) is straightforward. We want a function $u(r,\theta)=v(r)w(\theta)$ such that $v(r)$ satisfies

$$v(a)=v(b)=0, \qquad v'(a)=v'(b)=0, \tag{4.6}$$

and $w(\theta)$ satisfies

$$w(\phi)=w(\psi)=0, \qquad w'(\phi)=w'(\psi)=0; \tag{4.7}$$

and with our work from Chapter 3, we know just how to find such functions $v(r)$, $w(\theta)$. The boundary conditions (4.6) and (4.7) correspond with the boundary conditions (4.4) and (4.5), respectively.

Having our function $u(r,\theta)=v(r)w(\theta)$, we would like to approximate it using a Fourier series. Thus, we have

$$w^F(\theta)=\sum_{n=-\infty}^{\infty}a_ne^{in\theta}, \tag{4.8}$$

with the Fourier coefficients

$$a_n=\frac{1}{2\pi}\int_\phi^\psi w(\theta)e^{-in\theta}d\theta. \tag{4.9}$$

Thus, we have

$$u^F(r,\theta)=v(r)w^F(\theta)=v(r)\sum_{n=-\infty}^{\infty}a_ne^{in\theta}. \tag{4.10}$$

Then we would like to make our $u(r,\theta)$ a function of time so that we have our non-

propagating excitation orbit around the center of our annulus with angular frequency ω. Thus, we have

$$w^{TF}(\theta, t) = \sum_{n=-\infty}^{\infty} a_n e^{in(\theta - \omega t)} \tag{4.11}$$

so that

$$u^{TF}(r, \theta, t) = v(r) w^{TF}(\theta, t). \tag{4.12}$$

Having our time-dependent function $u^{TF}(r, \theta, t)$, we put it through the wave equation

$$\left[\nabla^2 - \frac{1}{c^2}\partial_{tt}\right] u(r, \theta, t) = -4\pi q(r, \theta, t) \tag{4.13}$$

to compute our force $q(r, \theta, t)$. And, for a fixed time t, we see what our force looks like for a corresponding nonpropagating excitation.

4.2 Computations

First, we define

$$v_m(r) = \begin{cases} c_m(r-K)^m + c_{m+2}(r-K)^{m+2} + c_{m+4}(r-K)^{m+4} & \text{if } r \in [a, b], \\ 0 & \text{otherwise} \end{cases} \tag{4.14}$$

with

$$K = \frac{a+b}{2}, \qquad c_m = c_{m+4}\frac{(a-b)^4}{16}, \qquad c_{m+2} = -c_{m+4}\frac{(a-b)^2}{2}, \qquad c_{m+4} = 1. \tag{4.15}$$

In all of our trials, we always have $b = 3$; but in some trials we have $a = 1$ and in others $a = 5/2$ to make our annulus as wide or narrow as we need it to be. Likewise, in some trials, $m = 0$; and in others, $m = 1$.

Next, we define

$$w_n(\theta) = \begin{cases} d_n(\theta-H)^n + d_{n+2}(\theta-H)^{n+2} + d_{n+4}(\theta-H)^{n+4} & \text{if } \theta \in [\phi, \psi], \\ 0 & \text{otherwise} \end{cases} \tag{4.16}$$

where

$$H = \frac{\phi + \psi}{2}, \qquad d_n = d_{n+4}\frac{(\phi - \psi)^4}{16}, \qquad d_{n+2} = -d_{n+4}\frac{(\phi - \psi)^2}{2}, \qquad d_{n+4} = 1. \tag{4.17}$$

In all of our trials, we always have $\phi = 0$; but we may have $\psi = \pi/2$ in some trials and $\psi = \pi/6$ in others so that we can have a larger or smaller sector angle as needed. Likewise, in some trials, $n = 0$; in others, $n = 1$.

Once we have our $w_n(\theta)$, we then compute its Fourier series

$$w_n^F(\theta) = \sum_{p=-N}^{N} \left(\frac{1}{2\pi} \int_{\phi}^{\psi} w_n(\theta') e^{-ip\theta'} d\theta' \right) e^{ip\theta}. \tag{4.18}$$

It is very important to get a very fine approximation of our $w_n(\theta)$, or else our contour plot of $q_{mn}(r, \theta, t)$ will come out with too many artifacts. So, in some trials, N can be as low as 6; and in other trials, N needs to be as high as 24.

At this point, we construct $u_{mn}(r, \theta) = v_m(r) w_n(\theta)$ and $u_{mn}^F(r, \theta) = v_m(r) w_n^F(\theta)$ and give their contour plots to make a comparison, as shown in Figure 4.1. Concerning the plots of this chapter, there are a couple of things we need to keep in mind. First, any white lines seen in our plots are artifacts. Secondly, when we talk about the plot of a function, we are actually talking about the plot of the real part of that function. So, in the case of $u_{mn}^F(r, \theta)$, Figure 4.1b is actually the plot of $\mathrm{Re}[u_{mn}^F(r, \theta)]$.

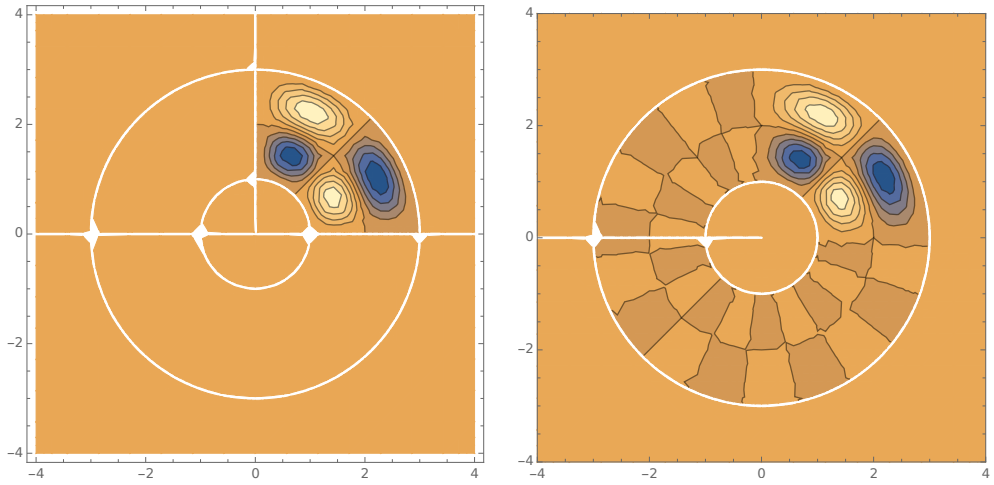

(a) (b)

Figure 4.1: (a) Our nonpropagating excitation compared with (b) its Fourier series. Here, $m = n = 1$.

Then we make a time-dependent version of $w_n^F(\theta)$. Thus we compute the Fourier series

$$w_n^{TF}(\theta, t) = \sum_{p=-N}^{N} \left(\frac{1}{2\pi} \int_{\phi}^{\psi} w_n(\theta') e^{-ip\theta'} d\theta' \right) e^{ip(\theta - \omega t)}, \tag{4.19}$$

where N is the same as in equation (4.18). Here we define $\omega = 2\pi$ so that our nonpropagating excitation goes around our annulus only once as our time t goes from 0 to 1.

And once we have our $w_n^{TF}(\theta, t)$, we define our now time-dependent nonpropagating excitation $u_{mn}^{TF}(r, \theta, t) = v_m(r) w_n^{TF}(\theta, t)$ and make contour plots of its real part for various values of t between 0 and 1 inclusive, watching our nonpropagating excitation go around the center of our annulus. And having our $u_{mn}^{TF}(r, \theta, t)$ and letting $c = 1$ be our wave speed, we put $u_{mn}^{TF}(r, \theta, t)$ through equation (4.13), the wave equation, to get our function $q_{mn}(r, \theta, t)$. Finally, we make contour plots of $q_{mn}(r, \theta, t)$ for various values of t between 0 and 1 inclusive. Figure 4.2 shows the real parts of our nonpropagating excitation and its corresponding force orbiting the center of our annulus.

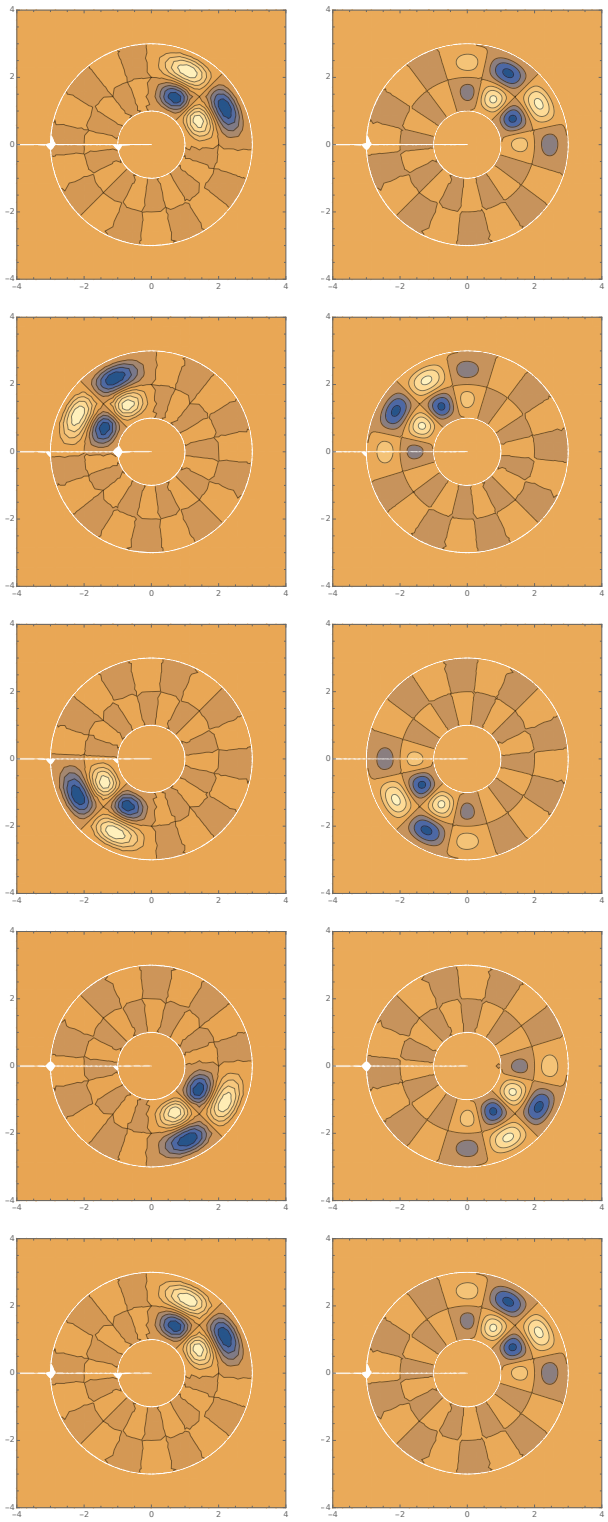

Figure 4.2: The left column shows our nonpropagating excitation $u_{11}^{TF}(r,\theta,t)$ orbiting the center of our annulus, and the right column shows the corresponding force $q_{11}(r,\theta,t)$ orbiting the same annulus. The first row corresponds to $t = 0$, the second to $t = 0.25$, the third to $t = 0.50$, the fourth to $t = 0.75$, and the fifth row to $t = 1$.

We followed this procedure for these four different functions: $u_{00}(r,\theta) = v_0(r)w_0(\theta)$, $u_{01}(r,\theta) = v_0(r)w_1(\theta)$, $u_{10}(r,\theta) = v_1(r)w_0(\theta)$, and $u_{11}(r,\theta) = v_1(r)w_1(\theta)$. Figure 4.3 gives the contour plots for all four of these functions, Figure 4.4 gives the contour plots for the time-dependent Fourier series of these functions, and Figure 4.5 gives the contour plots of the $q_{mn}(r,\theta,t)$'s resulting from our four $u_{mn}(r,\theta)$'s to be tested.

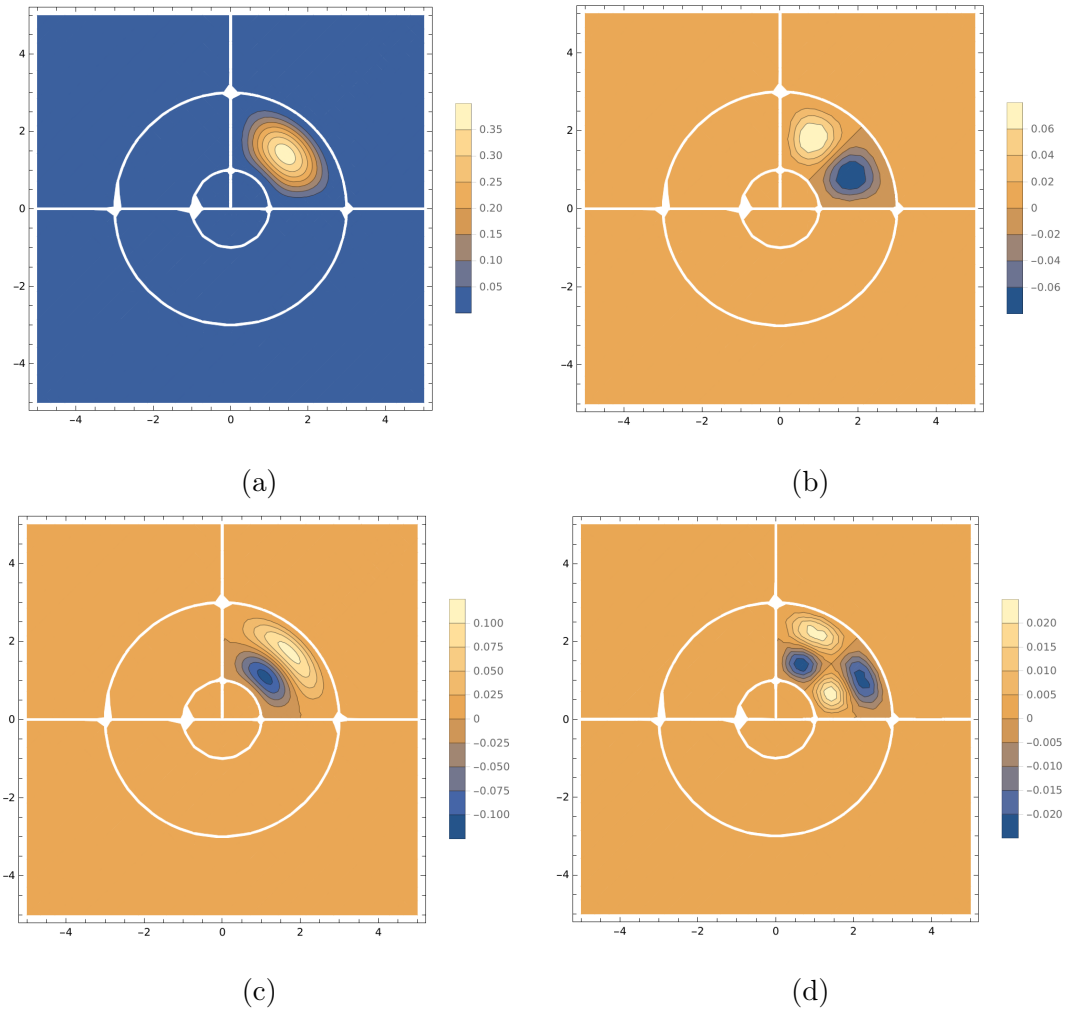

Figure 4.3: The plots of (a) $u_{00}(r,\theta)$, (b) $u_{01}(r,\theta)$, (c) $u_{10}(r,\theta)$, and (d) $u_{11}(r,\theta)$.

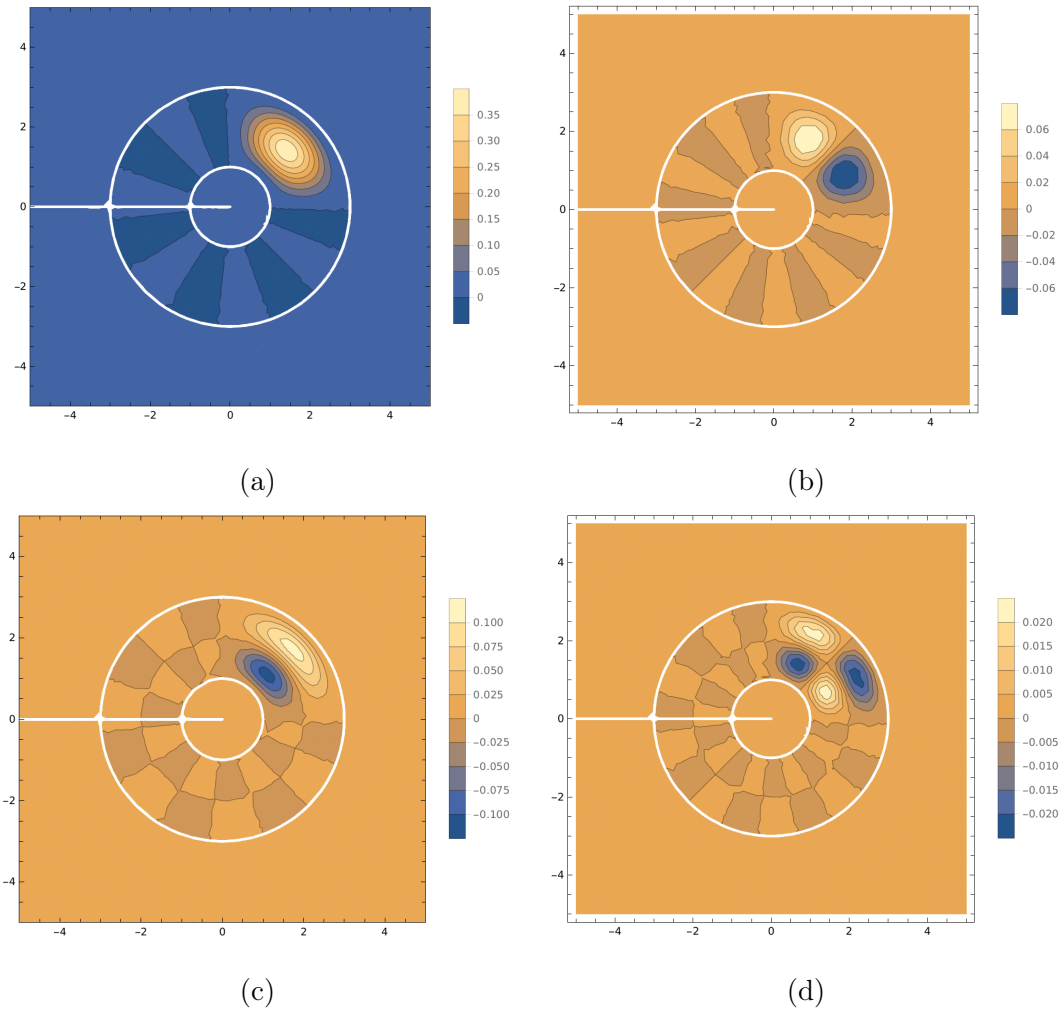

Figure 4.4: The plots of the time-dependent Fourier series of our nonpropagating excitations. Plotted are (a) $u_{00}^{TF}(r,\theta,t)$, (b) $u_{01}^{TF}(r,\theta,t)$, (c) $u_{10}^{TF}(r,\theta,t)$, and (d) $u_{11}^{TF}(r,\theta,t)$. At $t = 0$, the graph of each $u_{mn}^{TF}(r,\theta,t)$ above is identical with the graphs of the corresponding $u_{mn}^{F}(r,\theta)$.

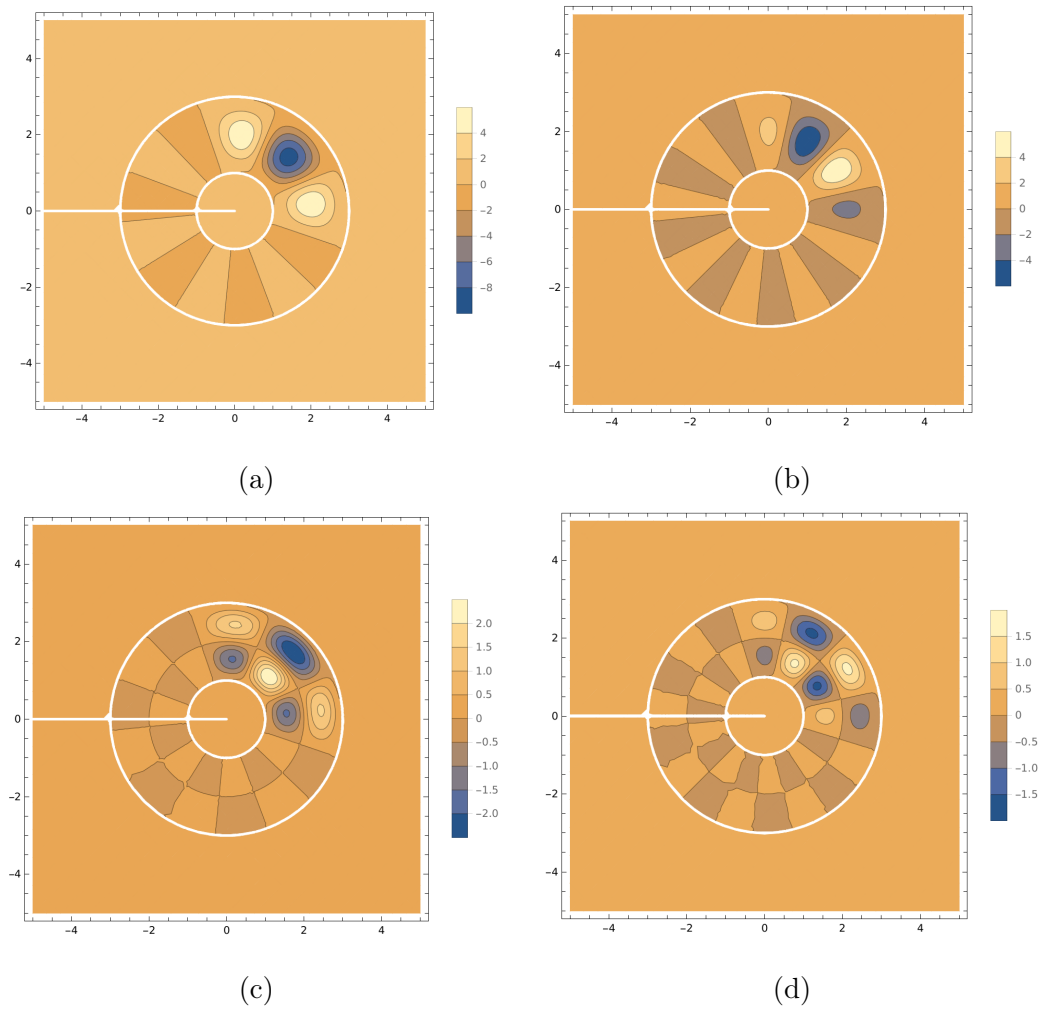

(a) (b)

(c) (d)

Figure 4.5: The plots of the forces corresponding with our nonpropagating excitations of Figure 4.3. Plotted are (a) $q_{00}(r,\theta,t)$, (b) $q_{01}(r,\theta,t)$, (c) $q_{10}(r,\theta,t)$, and (d) $q_{11}(r,\theta,t)$.

For all of our figures above, we had $a = 1$ and $\psi = \pi/2$. However, we tested our graphs with different values of a and ψ. All of these other trials with these other values of a and ψ produced more contour plots than we can illustrate here. So we will just leave it to Table 4.1 to give a summary of all of the different variables we tested for our experiment.

Table 4.1: All of the parameters tested in all of the trials of our experiment.

Trial No.	m	n	a	b	ϕ	ψ
1	0	0	1	3	0	$\pi/2$
2	0	0	1	3	0	$\pi/6$
3	0	0	5/2	3	0	$\pi/2$
4	0	0	5/2	3	0	$\pi/6$
5	0	1	1	3	0	$\pi/2$
6	0	1	1	3	0	$\pi/6$
7	0	1	5/2	3	0	$\pi/2$
8	0	1	5/2	3	0	$\pi/6$
9	1	0	1	3	0	$\pi/2$
10	1	0	1	3	0	$\pi/6$
11	1	0	5/2	3	0	$\pi/2$
12	1	0	5/2	3	0	$\pi/6$
13	1	1	1	3	0	$\pi/2$
14	1	1	1	3	0	$\pi/6$
15	1	1	5/2	3	0	$\pi/2$
16	1	1	5/2	3	0	$\pi/6$

We noticed three things in our results. First, most of the contour plots of this chapter, in particular the plots of Figures 4.4 and 4.5, look like the Rising Sun Flag or like dartboards. This dartboard pattern is a result of our use of the Fourier series to approximate $u_{mn}(r, \theta)$, as we can see from Figure 4.6.

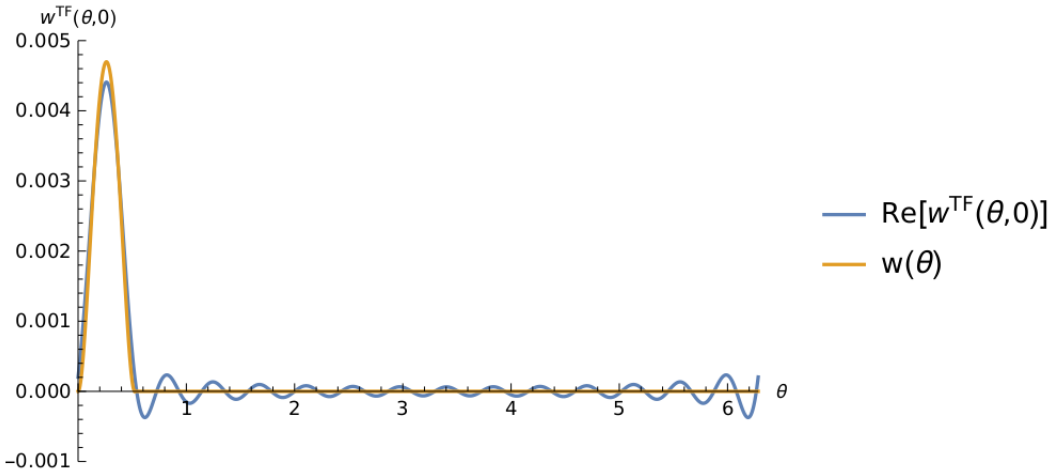

(a)

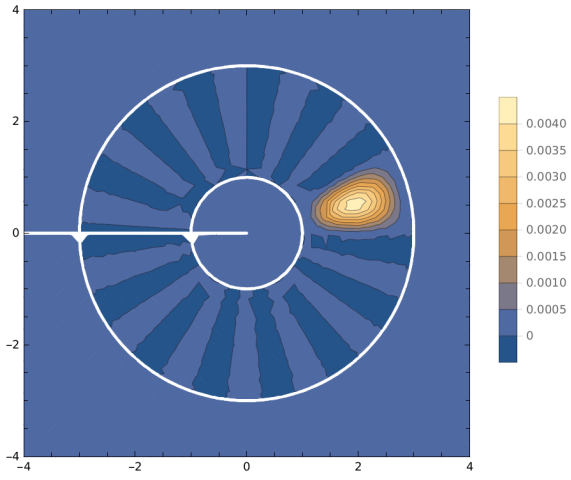

(b)

Figure 4.6: Our use of the Fourier series is why our contour plots look like dartboards. (a) The graph of the time-dependent $w_0^{TF}(\theta,t)$ and $w_0(\theta)$. The graph of $w_0^{TF}(\theta,t)$ ripples where the graph of $w_0(\theta)$ is perfectly flat. (b) The plot of $u_{00}^{TF}(r,\theta,t)$ exhibiting a dartboard pattern. Here, $a=1$, $\psi=\pi/6$, $m=n=0$, and $N=14$.

The second thing we noticed was that, for a given $u_{mn}(r,\theta)$, changing the size of the sector of our annulus did not change the basic form of our force $q_{mn}(r,\theta,t)$. For example, consider the forces $q_{00}(r,\theta,t)$ generated by the function $u_{00}(r,\theta)$ first in the case $a=1$, $\psi=\pi/2$ and then in the case $a=5/2$, $\psi=\pi/6$, as shown in Figure 4.7. (Remember, for all of our trials, we always had $b=3$, and $\phi=0$.) In the case of $a=5/2$, $\psi=\pi/6$, the form of $q_{mn}(r,\theta,t)$ is just like that of $q_{mn}(r,\theta,t)$ in the case of

$a = 1$, $\psi = \pi/2$ except that $q_{mn}(r, \theta, t)$ is "squished" into a smaller area in the case of $a = 5/2$, $\psi = \pi/6$. So what this tells us is that we can make our sector whatever shape we want or as small as we want and still have a nonpropagating excitation.

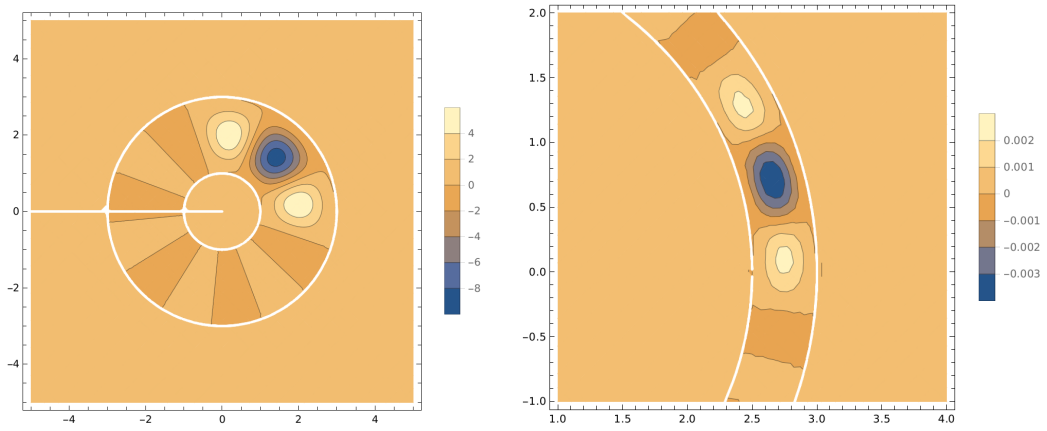

(a) (b)

Figure 4.7: Our force $q_{00}(r, \theta, t)$ on two different sectors of our annulus. (a) The sector of our annulus with $a = 1$ and $\psi = \pi/2$, and (b) a close-up of the sector of our annulus with $a = 5/2$ and $\psi = \pi/6$.

And finally, the third thing we noticed is that there appear to be equal amounts of positive and negative force in the plots of our forces. This makes sense because the destructive interference that makes our nonpropagating excitations nonpropagating is apparently created by a cancellation of waves from positive and negative sources.

CHAPTER 5: CONCLUSIONS

Thus, we have managed to construct two-dimensional nonpropagating excitations, even two-dimensional nonpropagating excitations that orbit, exhibiting translational motion. We can even construct orbiting two-dimensional nonpropagating excitations on as small a sector of an annulus as we would like. From here, we ought to be able to construct 2-D nonpropagating excitations that move in other motions like a figure eight pattern or a square pattern. The new nonpropagating excitations considered in this thesis were general, not applied to any particular branch of physics. Similar nonpropagating excitations should exist for electromagnetic waves and gravitational waves, which can all be reduced in special cases to wave equations with a source term.

REFERENCES

[1] G. Gbur, "Nonradiating sources and other 'invisible' objects," *Progress in Optics*, 2003.

[2] G. Gbur, *Nonradiating Sources and the Inverse Source Problem*. PhD thesis, University of Rochester, 2001.

[3] P. Ehrenfest, "Asymmetric power movement without magnet or radiation fields," *Physikalische Zeitschrift*, 1910.

[4] G. A. Schott, "The electromagnetic field of a moving uniformly and rigidly electrified sphere and its radiationless orbits," *Philosophical Magazine*, pp. 752–761, 4 1933.

[5] D. Bohm and M. Weinstein, "The self-oscillations of a charged particle," *Physical Review*, pp. 1789–1798, 12 1948.

[6] G. H. Goedecke, "Classically radiationless motions and possible implications for quantum theory," *Physical Review*, pp. B281–B288, 7 1964.

[7] F. G. Friedlander, "An inverse problem for radiation fields," *Proceedings of the London Mathematical Society*, no. 3, pp. 551–576, 1973.

[8] A. J. Devaney and E. Wolf, "Radiating and nonradiating classical current distributions and the fields they generate," *Physical Review*, pp. 1044–1047, 8 1973.

[9] N. Bleistein and J. K. Cohen, "Nonuniqueness in the inverse source problem in acoustics and electromagnetics," *Journal of Mathematical Physics*, pp. 194–201, 2 1977.

[10] D. Moses, C. H. Gan, and G. Gbur, "Directional, nonpropagating, and polychromatic excitations in one-dimensional wave systems," *Physical Review*, no. 2, 2009.

[11] M. Berry, J. T. Foley, G. Gbur, and E. Wolf, "Nonpropagating string excitations," *American Journal of Physics*, pp. 121–123, 2 1998.

[12] G. Gbur, J. T. Foley, and E. Wolf, "Nonpropagating string excitations–finite length and damped strings," *Wave Motion*, pp. 125–134, 9 1999.

[13] N. A. Nemkov, I. V. Stenishchev, and A. A. Basharin, "Nontrivial nonradiating all-dielectric anapole," *Scientific Reports*, 2017.

[14] K. Koshelev, G. Favraud, A. Bogdanov, Y. Kivshar, and A. Fratalocchi, "Nonradiating photonics with resonant dielectric nanostructures," *Nanophotonics*, pp. 725–745, 5 2019.

[15] G. Labate, A. K. Ospanova, N. A. Nemkov, A. A. Basharin, and L. Matekovits, "Nonradiating anapole condition derived from devaney-wolf theorem and excited in a broken-symmetry dielectric particle," *Optics Express*, pp. 10294–10307, 3 2019.

[16] P. M. Morse and K. U. Ingard, *Theoretical Acoustics*. Princton University Press, 1986.

[17] G. Gbur, *Mathematical Methods for Optical Physics and Engineering*. Cambridge University Press, 2011.

[18] G. Gbur, "Computational Helmholtz." This is a scan of handwritten notes., 6 2014.

APPENDIX: WHEN THE HANKEL FUNCTION'S ARGUMENT IS ZERO

The discussion that follows comes from [18].

We start off with our Helmholtz equation

$$\left[\nabla^2 + k^2\right] u(\mathbf{r}) = -4\pi q(\mathbf{r}), \tag{A.1}$$

whose solution is the Green's formula

$$u(\mathbf{r}) = \int_D G(\mathbf{r}, \mathbf{r}') q(\mathbf{r}') d^2\mathbf{r}', \tag{A.2}$$

where D is the region of integration and G is a Green's function. The way we compute equation (A.2) is that we discretize our region D into smaller sections D_j so that $D = \bigcup_j D_j$, and we compute

$$u(\mathbf{r}_i) = \sum_j \int_{D_j} G(\mathbf{r}_i, \mathbf{r}') q(\mathbf{r}') d^2\mathbf{r}'. \tag{A.3}$$

Now, when $j \neq i$, we treat the terms in our summation approximately as constants. On the other hand, when $j = i$, we treat these terms separately. Thus, we end up with

$$u(\mathbf{r}_i) = \sum_{j \neq i} G(\mathbf{r}_i, \mathbf{r}_j) q(\mathbf{r}_j) \Delta A + q(\mathbf{r}_i) \int_{D_i} G(\mathbf{r}_i, \mathbf{r}') d^2\mathbf{r}', \tag{A.4}$$

where ΔA is the area of the region D_j.

In 2-D, we have that $G(\mathbf{r}_i, \mathbf{r}_j) = i\pi H_0^{(1)}(k|\mathbf{r}_i - \mathbf{r}_j|)$, where $H_0^{(1)}$ is a Hankel function. So, if we wrote equation (A.4) only as

$$u(\mathbf{r}_i) = \sum_j G(\mathbf{r}_i, \mathbf{r}_j) q(\mathbf{r}_j) \Delta A, \tag{A.5}$$

in those moments when $i = j$, the argument of our Hankel function would become zero, which would make the Hankel function blow up. Here, we come up with a way around this problem.

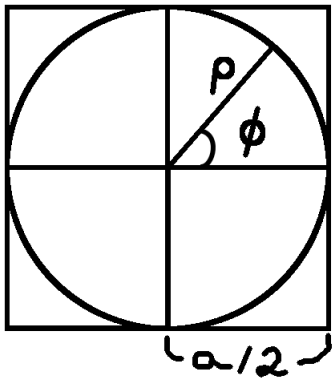

Figure 1: Our region D_j. Here, a is the length of the side of our region and ϕ is the angle ρ makes with the x-axis.

So we want to compute the term $\int_{D_i} G(\mathbf{r}_i, \mathbf{r}')d^2\mathbf{r}'$ of equation (A.4). Thus, we define

$$Q = \frac{1}{a^2}\int_{D_i} G(\mathbf{r}_i, \mathbf{r}')d^2\mathbf{r}'. \tag{A.6}$$

Let $G = i\pi H_0^{(1)}(k\rho)$. We will get to the purposes of a and ρ in a moment. Assymptotically, we have

$$H_0^{(1)}(k\rho) \sim \sqrt{\frac{2}{\pi k\rho}} \tag{A.7}$$

so that

$$G \sim i\sqrt{\frac{2\pi}{k\rho}}. \tag{A.8}$$

Thus,

$$\begin{aligned} Q &= i\frac{\sqrt{2\pi}}{k}\frac{1}{a^2}\int_0^{\rho(\phi)}\int_0^{2\pi}\frac{1}{\rho^{1/2}}\rho d\rho d\phi \\ &= 4i\sqrt{\frac{2\pi}{k}}\frac{1}{a^2}\int_{-\pi/4}^{\pi/4}\frac{2}{3}(\rho(\phi))^{3/2}d\phi \\ &= \frac{8i}{3}\sqrt{\frac{2\pi}{k}}\frac{1}{a^2}\int_{-\pi/4}^{\pi/4}(\rho(\phi))^{3/2}d\phi. \end{aligned} \tag{A.9}$$

Let a be the length of the side of the square region D_j, let ρ be the radius of the circle in Figure 1, and let ϕ be the angle between the x-axis and the segment whose length is ρ, as shown in Figure 1. We have that

$$\cos\phi = \frac{a}{2\rho(\phi)} \tag{A.10}$$

so that

$$\rho(\phi) = \frac{a}{2\cos\phi}. \tag{A.11}$$

Thus,

$$Q = \frac{8i}{3\sqrt{8}}\sqrt{\frac{2\pi}{ka}}\int_{-\pi/4}^{\pi/4}(\cos\phi)^{-3/2}d\phi, \tag{A.12}$$

where, using *Mathematica*, we have that

$$\int_{-\pi/4}^{\pi/4}(\cos\phi)^{-3/2}d\phi = 1.875. \tag{A.13}$$

Thus,

$$Q = \frac{4i}{3}\sqrt{\frac{\pi}{ka}}(1.875) = \frac{4.43i}{\sqrt{ka}}. \tag{A.14}$$

Making the appropriate substitutions, we have

$$u(\mathbf{r}_i) = \sum_{j\neq i} G(\mathbf{r}_i,\mathbf{r}_j)q(\mathbf{r}_j)a^2 + q(\mathbf{r}_j)Qa^2, \tag{A.15}$$

where we make the substitution

$$G(\mathbf{r}_i,\mathbf{r}_j) = \begin{cases} G(\mathbf{r}_i,\mathbf{r}_j) & \text{for} \quad i \neq j, \\ Q & \text{for} \quad i = j. \end{cases} \tag{A.16}$$

Note that in equation (A.15), where we once had ΔA as in equation (A.4), we now have a^2.